Journal for Multiscale Computational Engineering, 12 (4): 271–289 (2014)

NONLINEAR MULTISCALE HOMOGENIZATION OF CARBON NANOTUBE REINFORCED COMPOSITES WITH INTERFACIAL SLIPPAGE

Dimitris Savvas & Vissarion Papadopoulos*

Institute of Structural Analysis and Antiseismic Research, National Technical University of Athens, 9 Iron Polytechneiou, Zografou Campus, Athens 15780, Greece

*Address all correspondence to Dimitris Savvas, E-mail: dimitriosavvas@yahoo.gr

A nonlinear hierarchical multiscale approach is proposed in this work, for the characterization of the mechanical and damping properties of carbon nanotube reinforced composites (CNT-RCs) considering slippage at CNT/polymer interface. The proposed numerical strategy encompasses various length scales, from nano to micro to macro. Individual CNTs are modeled at the nanoscale as space frame structures using the modified Molecular Structural Mechanics (mMSM) approach. Then the mMSM model is projected to an equivalent continuum beam element (EBE) which is subsequently used as the basic building block for the construction of full length straight CNTs at the microscale, embedded in a polymer matrix. The interfacial load transfer mechanism between the lateral surface of the CNT and the surrounding polymer is modeled with a nonlinear bond-slip friction-type model. This scheme provides with the finite element model of a Representative Volume Element (RVE) at the microscale in which a nonlinear homogenization scheme is implemented in order to compute effective material properties for the macrocontinuum. A Hill's anisotropic plasticity model is fitted onto the results of finite element analysis of the microstructured RVE model, so that anisotropic stiffness and energy dissipation mechanism, due to the directionality of the CNTs, can be captured by the equivalent macro model. Sensitivity analysis is performed with respect to various weight fractions (wf) of CNTs and interfacial shear strength (ISS) values. Global mechanical and damping properties for the homogenized models are assessed and compared with direct calculations on detailed fine scale models.

KEY WORDS: *molecular structural mechanics, multiscale modeling, homogenization, carbon nanotubes, nanocomposites, Hill's plasticity*

1. INTRODUCTION

Since the discovery of carbon nanotubes (CNTs) by Iijima (1991) intensive research effort has been conducted on the development of advanced CNT-reinforced composites (CNT-RCs) (Andrews and Weisenberger, 2004; Lau and Hui, 2002; Thostenson et al., 2005; Wang et al., 2011). Considering the superior mechanical properties of single or multi-walled CNTs, often reported in experimental (Demczyk et al., 2002; Salvetat et al., 1999; Xu et al., 2006; Yuen et al., 2007) as well as in numerical studies (Arroyo and Belytschko, 2004; Chang and Gao, 2003; Jin and Yuan, 2003; Li and Chou, 2003a), combined with their relatively small diameter, high aspect ratio, and large surface area, their potential to be used as reinforcement fillers in polymer matrix composites is fully attractive. Qian et al. (2000) reported 36–42 and $\sim$25% increases in elastic modulus and ultimate stress of a composite film, respectively, with only 1% wf of CNTs. Other researchers however demonstrated a modest improvement in strength and stiffness of CNT-RCs, claiming that CNTs alignment, dispersion and geometry could significantly affect the final composite properties (Chen and Tao, 2006; Namilae and Chandra, 2005). An important factor which also influences the behavior of the CNT-RCs is the CNT/polymer interface. Interfacial properties as well as their effect on the overall stiffness of the nanocomposites have been mainly investigated numerically in the context of molecular dynamics (MD) simulations (Frankland et al.,

1543–1649/14/$35.00

2002; Griebel and Hamaekers, 2004; Han and Elliott, 2007; Yang et al., 2005). In addition, the important role of functionalization, a chemical process applied on the surface of CNTs for enhancing the load transferring mechanisms at the interface, has been demonstrated in various experimental (Schadler et al., 1998; Shen et al., 2007; Wang et al., 2008) and numerical works (Hou et al., 2009; Park et al., 2006; Savvas et al., 2012).

MD simulations, despite their ability to accurately represent phenomena taking place at the nanoscale, cannot be applied at larger scales and representative time spans, due to limitations of the available computer power resources. To overcome the aforementioned restrictions continuum-based mechanics approaches emerged as alternatives capable of modeling larger scale systems and longer time spans. These methods have been applied in order to predict equivalent mechanical properties for CNTs. Li and Chou (2003a) introduced the molecular structural mechanics approach (MSM), which is based on energy equivalence between molecular and continuum mechanics. The proposed method was used for the analysis of CNTs where the carbon–carbon (C–C) covalent bonds of the lattice structure were substituted by representative continuum round profile beams. A modified (mMSM) version of the MSM approach was proposed by Chen et al. (2010) and accounts for different bending rigidities along the major and minor principal axes of representative rectangular beams. Various atomic force field potentials such as quadratic, Morse, or Lennard-Jones have been also used in the framework of MSM to account for linear and nonlinear covalent bonds as well as noncovalent van der Waals interactions (Arroyo and Belytschko, 2004; Li and Chou, 2003b; Xiao et al., 2005). It must be noted that molecular mechanics is essentially an interpolation scheme, the success of which depends not only on good estimation of force field parameters, but also on systematics among related molecules (Hehre, 2003). For carbon nanotubes for which MSM cannot be applied, such as boron nitride and molybdenum, more accurate quantum models based on atomistic calculations need to be used (Dumitrica et al., 2003; Zhang and Dumitrica, 2008).

In the context of CNT-RC modeling where different length scales are coupled and atomic interactions at the interface of the constituents are taking place, multiscale methods are regarded as the ultimate analysis tool (Weinan et al., 2007). Concurrent, semi-concurrent, and serial coupling multiscale methodologies are among the most widely applied. In the concurrent approach strong coupling between the lower and upper scales is satisfied by so-called bridging scales methods (Qian et al., 2008; Wernik and Meguid, 2009). In these approaches, the solution of the atomistic problem provides the boundary conditions or kinematic constraints that must be imposed to the continuum problem. In semi-concurrent methods a weaker coupling is imposed by recovering the stress–strain law at each Gauss-point from the solution of a boundary value problem of a corresponding RVE. The boundary value problems at the upper–lower scales have to be addressed simultaneously by nested solvers, usually named after FE^2 solution (Kouznetsova et al., 2004; Miehe and Koch, 2002). Both concurrent and semi-concurrent methods are particularly suitable for capturing evolving nonlinear microstructural phenomena during loading of the macrostructure, such as damage or fracture. However, these methods pose severe limitations when dealing with large-scale applications which involve complex microstructure topologies, due to the fact that they are extremely computational intensive.

Serial coupling approaches apply a length separation and the problem is efficiently solved hierarchically form the smallest scale passing information to its subsequent scale and onwards (van der Sluis et al., 1999). A key issue in these methods is the definition of appropriate interscale relations which describe the macroscopic deformation behavior from the microstructural phenomena. As a first step in the hierarchical multiscale analysis of CNT-RCs, effective material properties for the individual CNTs have to be defined. These are usually calculated using MD or MSM simulations and thus projected to equivalent continuum elements. Subsequently, the overall equivalent constitutive behavior of the composite is estimated using analytical micromechanics-based models or numerical homogenization techniques. In this framework, Odegard et al. (2003) suggested an effective continuum fiber to model the CNT, the local polymer near the CNT, and the CNT/polymer interface, based on molecular mechanics and equivalent continuum modeling. Next, by applying a Mori–Tanaka analytical model, effective elastic properties for composites with aligned and misaligned CNTs were calculated. Spanos and Kontsos (2008) presented a stochastic multiscale homogenization procedure to model the spatial variability of the CNTs volume fraction and quantify its effect on the mechanical properties of the composite. In Seidel and Lagoudas (2006) a hierarchial multiscale model is proposed combining the layered composite cylinder approach, used for the CNT modeling, with Mori–Tanaka and self-consistent homogenization, in an attempt to consider CNT clustering effect in the calculations of the CNT-RC's effective properties. Similarly, in Yang et al. (2012) a sequential multiscale bridging model was developed to account for the CNT size effect and weakened bonding effect at the interface through MD simulations and continuum micromechanics.

In the present work a nonlinear multiscale homogenization methodology is proposed for the characterization of the mechanical and damping properties of CNT-RCs. The novelty of the proposed multiscale approach is that it combines different modeling strategies in order to accurately pass information between scales. This hierarchical approach is demonstrated in Fig. 1 where the modeling steps from nano to micro to macro scale are depicted. Short length CNTs are modeled at the nano scale as space frame structures using the mMSM approach where the C–C covalent bonds of the lattice are substituted by rectangular beams. Since CNTs form "ropes" in the order of micrometers, the aforementioned short length CNT model is projected to a linear EBE which is subsequently used as the basic building block for the modeling of long straight CNTs at the microscale which are embedded in the polymer matrix. The interfacial load transfer mechanism between the lateral surface of the CNT and the surrounding polymer is modeled with a nonlinear bond-slip friction-type model. This bond-slip model is particularly suitable for modeling the stick–slip behavior observed in functionalized CNTs in which a chemical treatment onto their surface has been applied in order to form covalent bonds with the hyperbranched polymers. In that way a significant increase of the interfacial shear strength (ISS) between the CNT and the matrix may be achieved (Barber et al., 2003; Frankland et al., 2002).

A nonlinear homogenization scheme is finally implemented in order to compute effective material properties. This is accomplished by applying appropriate displacement-type boundary conditions on the previously described micromechanical RVE model, which correspond to prescribed macrostrain tensors. The resulting macrostress tensors are computed from FE analyses of the RVE in a volume average manner. A phenomenological constitutive model based on Hill's anisotropic plasticity is adjusted to the macrocontinuum body through the proposed homogenization method, in order to account for the anisotropic stiffness and energy dissipation mechanism of the CNT-RC. This anisotropy is physically induced by the directionality of the CNTs inside the polymer matrix. Specifically, the initial yield stress and the kinematic hardening data are extracted from the nonlinear homogenization step and assigned to the macro constitutive Hill's plasticity model in order to predict stress–strain hysteresis loops under cycling load. Validation of the proposed homogenization approach is performed on the basis of sensitivity analysis on RVEs with respect to various weight fractions of CNTs and interfacial shear strength values. In addition, global mechanical and damping properties for the homogenized models are assessed and compared with direct calculations on detailed fine scale models.

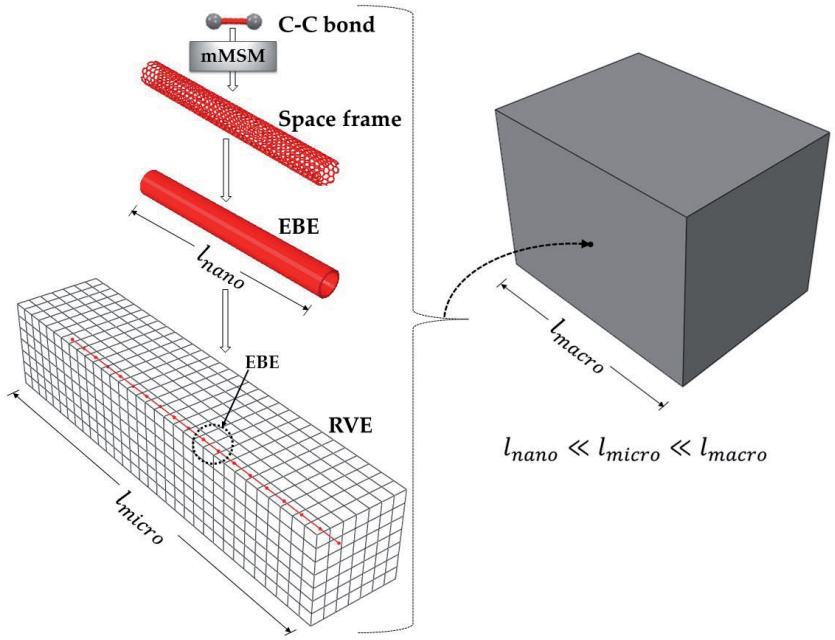

FIG. 1: Hierarchical multiscale homogenization step.

2. MICROSTRUCTURED MULTISCALE MODEL

The microstructured model of Fig. 1 is constructed following a sequential multiscale approach in which, at the lowest scale, the interatomic relations between carbon atoms are governed by a quadratic force field potential. Using the mMSM approach the C–C covalent bonds are substituted by continuum beam elements allowing the atomic lattice of the nanotube to be modeled as a space frame structure at the nanoscale. Proceeding to the next scale, the space frame is reduced to an equivalent beam element (EBE) which is the structural element in the chain construction of long straight micro CNT "ropes." The final microstructured RVE model is formulated by embedding these equivalent beam elements into the finite element discretized bulk matrix. A brief description of the multiscale modeling steps, followed for the discretization of the microstructured RVE model, is given below. A more detailed description of this model can be found in Savvas et al. (2012).

2.1 Modified Molecular Structural Mechanics Approach

The molecular structural mechanics approach and its modified version (mMSM) used here, belongs to the equivalent continuum modeling (ECM) approaches which tend to be a more efficient modeling strategy for simulating larger scale systems and longer time spans compared to *ab initio* or other molecular dynamics (MD) simulations. The core principle in these methods is to establish a linkage between molecular and structural mechanics, based on systems energy equivalence developed due to chemical bonds between carbon–carbon atoms (C–C) and the strain energy of a solid beam element following by continuum mechanics. Thus, having adopted a quadratic potential force field to account for linear covalent C–C interactions and a rectangular beam element in the context of finite element method, the following relationships between structural mechanics parameters and molecular mechanics force field constants are derived:

$$k_r = \frac{EA}{L}, \quad k_\theta = \frac{E\left(I_y'' + I_z\right)}{L}, \quad k_\omega = \frac{3EI_y'}{L}, \quad k_\tau = \frac{GJ}{L} \tag{2.1}$$

$$I_y = I_y' + I_y'' = \left(\frac{k_\omega}{3k_\theta} + tan\phi\right) I_z \tag{2.2}$$

These expressions relate the axial, bending, and torsional rigidities of the equivalent rectangular beam to known force field constants k_r, k_θ, k_ω, and k_τ which are the bond-stretching, bond-angle variation, inversion, and torsional-resistance force constants, respectively. Notice that in mMSM approach different bending rigidities are assigned along the major and minor principal axes of the considered rectangular beam. A detailed description of the mMSM approach can be found in Chen et al. (2010).

2.2 EBE

The implementation of mMSM approach mentioned above leads to a space frame model which reprsents the atomic lattice of the nanotube. Although this modeling technique overcomes the restrictions in time and size-scales of MD, the detailed simulation of the entire nanostructure of a CNT leads to a large-scale computational problem difficult to handle as well. For this reason, a portion of the detailed space frame structure of the CNT's lattice is projected to an EBE. Linear material properties are assigned to this EBE through finite element simulations of tension, bending and torsion performed on the mMSM model. Figure 2 depicts the applied displacement boundary conditions u_x, u_y, ϕ and the corresponding reaction forces. The axial, bending, and torsional rigidities of the EBE are calculated by the following equations:

$$(EA)_{eq} = \frac{F_x L_0}{u_x}, \quad (EI)_{eq} = \frac{F_y}{3u_y} L_0^3, \quad (GJ)_{eq} = \frac{T}{\phi} L_0 \tag{2.3}$$

2.3 Construction of RVE

As previously mentioned, individual CNTs are modeled as a series of EBEs forming long CNT "ropes" with lengths in the microscale. Then the RVE for a material point of the homogeneous CNT-RC can be constructed as a statistically

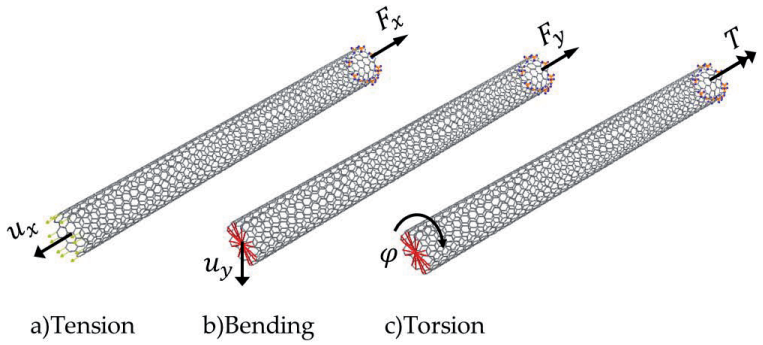

FIG. 2: FE mesh and boundary conditions for **(a)** Tension, **(b)** Bending, and **(c)** Torsion of CNT's space frame model.

representative material volume of the microstructure. In this study straight CNTs are embedded in a bulk matrix and are considered fully aligned and oriented. As described in detail in Savvas et al. (2012), the embedded finite element technique is used, in order to avoid complicated mesh configurations for the RVE. Thus, the RVE FE model consists of 3D Bernoulli beam elements for the modeling of CNTs and 8-noded solid elements for the matrix. Linear material properties are assigned to both CNTs and matrix. The hierarchical modeling steps followed from the individual CNT simulation to the construction of the CNT-RC's RVE are depicted in Fig. 1.

2.4 Bond-Slip Model

Mechanical and damping properties of the nanocomposites are sensitive to the interfacial characteristics between the CNT and the matrix. Especially, the functionalized CNTs considered in this study display an improved interaction with the polymer matrix. Functionalization of CNTs is a chemical process that requires severe treatments of oxidation in order to generate functional groups in the surface or ends of the CNTs. After this process covalent bonds are formed onto the CNT's surface with hyperbranched polymers. As reported in Frankland et al. (2002), if only 1% of the carbon atoms are covalently bonded to that of the polymer, the ISS can be increased up to one order of magnitude. Therefore in case of functionalized CNTs, weak vdW interactions can be omitted from the modeling procedure, since the dominant mechanism of the load transferring between the polymer and the nanotube is mechanical interlocking. Pullout tests conducted on CNT-RCs (Barber et al., 2003; Ganesan et al., 2011) revealed a stick-slip behavior of CNTs inside the matrix. According to these experiments, a full bonded behavior is observed between the CNT and the polymer, until a critical ISS value is reached, after which slippage is initiated. For this reason, a nonlinear friction-type bond-slip model is incorporated in the FE analysis of the microstructured RVE. With reference to Fig. 3 the equilibrium equation for a CNT's EBE i leads to the following slippage criterion:

$$\tau_i = \frac{A_i}{\pi(D_i + t_i)l_i} |\sigma_{Ri} - \sigma_{Li}| \begin{cases} < ISS, & \text{fully bonded} \\ \geq ISS, & \text{slip} \end{cases} \tag{2.4}$$

where τ_i is the calculated interfacial shear stress, A_i is the cross-sectional area of the EBE, which has an outer diameter $D_i + t_i$ and length l_i. The nodal axial stresses σ_{Ri} and σ_{Li} acting on the right and left end section of EBE i, are derived after a smoothing procedure as

$$\sigma_{Ri} = \frac{\sigma_i l_i + \sigma_{i+1} l_{i+1}}{l_i + l_{i+1}}, \qquad \sigma_{Li} = \frac{\sigma_i l_i + \sigma_{i-1} l_{i-1}}{l_i + l_{i-1}} \tag{2.5}$$

So, if an EBE representing some portion of the full length CNT "rope" is in slip state, then its corresponding interface bond has failed and no further load transferring is allowed. The condition of slip for an EBE is simulated by a damage model which reduces its axial stiffness to a very small value. Bending and torsion rigidities are not affected by this

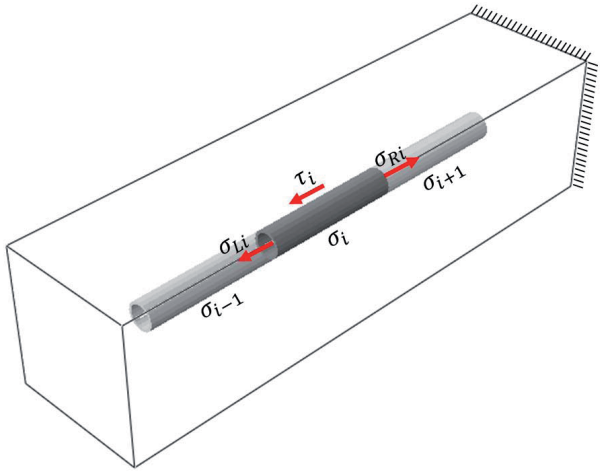

FIG. 3: Equilibrium of an EBE.

modeling, allowing the element which is in slip state to resist against bending and torsion. This slip model is implemented within a full Newton–Raphson incremental-iterative scheme for the solution of the resulting FE nonlinear equations. The basic steps of the algorithm are summarized below.

Step 1: Compute the incremental displacements ${}^t\Delta u^{(i)}$ at increment t and iteration i due to the increment ${}^t\Delta P$ of the external load vector

$$ {}^t\Delta u^{(i)} = \left[{}^tK_T^{(i)} \right]^{-1} {}^t\Delta P \tag{2.6} $$

Step 2: Loop over all beam elements and check each element e for slippage

$$ \text{Slippage} \begin{cases} \text{no} \rightarrow & {}^tK_{Te}^{(i)} = {}^tK_{Te}^{(i-1)} \\ \text{yes} \rightarrow & {}^tK_{Te}^{(i)} = {}^tK_{Te}^{(i-1)}, \text{with } (EA)_e \rightarrow 0 \end{cases} \tag{2.7} $$

when slippage occurs, the axial stiffness is reduced to zero, resulting in a local modified tangent stiffness matrix ${}^tK_{Te}^{(i)}$

Step 3: Correction of internal forces ${}^t\Delta F_e^{(i)}$ of element e and update global force vector ${}^tF^{(i)}$

$$ {}^t\Delta F_e^{(i)} = {}^tK_{Te}^{(i)} \Delta u_e^{(i)} \tag{2.8} $$

$$ {}^tF^{(i)} = {}^tF^{(i-1)} + \sum_{e=1}^{N} {}^t\Delta F_e^{(i)} \tag{2.9} $$

Step 4: Compute the residuals ${}^tr^{(i)}$

$$ {}^tr^{(i)} = {}^tP - {}^tF^{(i)} \begin{cases} \leq tol \;\; \text{then} \;\; t = t+1 & \text{go to next increment} \\ > tol \;\; \text{then} \;\; i = i+1 & \text{go to } \textbf{Step 1} \end{cases} \tag{2.10} $$

3. NONLINEAR HOMOGENIZATION

The homogenization scheme adopted in this paper belongs to the family of hierarchical computational homogenization methods for which the microscopic behavior of the heterogeneous medium is projected to an homogeneous equivalent continuum model at an upper scale. Thus, a specific constitutive material behavior has to be identified via FE analysis of the microstructured model and assigned to the macrocontinuum. The fundamental assumption in such homogenization procedures is the statistical homogeneity of the heterogenous medium (Hashin, 1983), which means that all statistical properties of the state variables are the same at any material point and thus a representative volume element (RVE) can be recognized. With this approach, relations between microscopic and macroscopic state variables (e.g., stresses and strains) are extracted by imposing appropriate boundary conditions on the RVE, necessary to determine the constitutive parameters for the material of the equivalent homogeneous continuum.

The first step in the homogenization procedure is to define the relations between the microscopic and macroscopic state variables which are known as micro–macro relations. As mentioned, macroscopic quantities are formulated as volume averages of the corresponding microscopic state variables. According to the deterministic theories of Hill (1963) and Maugin (1992), the total macroscopic stress and strain tensors at some point $\boldsymbol{X}$ of the continuum body are computed by

$$\Sigma_{ij}(\boldsymbol{X}) = \langle \sigma_{ij} \rangle (\boldsymbol{X}), \qquad E_{ij}(\boldsymbol{X}) = \langle \varepsilon_{ij} \rangle (\boldsymbol{X}) \tag{3.1}$$

where the average of a quantity ψ at the microstructure is defined as its integral over the corresponding RVE volume V as

$$\langle \psi \rangle (\boldsymbol{X}) = \frac{1}{V} \int_R \psi(\boldsymbol{X}, \boldsymbol{Y}) \, \mathrm{d}\boldsymbol{Y} \quad \text{with} \quad V = \int_R \mathrm{d}\boldsymbol{Y} \tag{3.2}$$

where $\boldsymbol{Y}$ denotes the coordinate system in the microstructured RVE. The averaging theorem requires the strain energy of the the microstructured RVE to be equal to that of the homogenized macrocontinuum. This equivalence is represented by the following equation:

$$\boldsymbol{\Sigma} : \boldsymbol{E} = \frac{1}{|V|} \int_R \boldsymbol{\sigma} : \boldsymbol{\varepsilon} \, \mathrm{d}\boldsymbol{Y} \tag{3.3}$$

3.1 Anisotropic Hill's Plasticity Model: Basic Equations

Heterogeneous materials used in engineering practice usually exhibit anisotropic elastic and plastic properties. Specifically, composites with reinforcements oriented in predefined directions, display orthotropic elastoplastic behavior. Such inherent anisotropy in materials cannot be adequately described by the von Mises criterion which is based on isotropic yielding. An extension of the standard von Mises model was proposed by Hill (1950) in order to simulate orthotropic plasticity often found in formed steel.

In the present paper, Hill's orthotropic plasticity model is adopted and incorporated in the hierarchical homogenization procedure in order to capture the anisotropy induced by the CNT's orientation. First we assume that the material possesses three orthogonal axes (see Fig. 4) which remain constant during the course of plastic deformations. Thus the stress tensor components σ_{ij} can be expressed on an orthonormal basis $\{e_1, e_2, e_3\}$ whose vectors coincide with the principal axes of transversal orthotropy.

The yield function associated with Hill's model can be written in the form:

$$\Phi(\boldsymbol{\sigma}, \overline{\sigma}) = F(\sigma_{22} - \sigma_{33})^2 + G(\sigma_{33} - \sigma_{11})^2 + H(\sigma_{11} - \sigma_{22})^2 + 2L\sigma_{23}^2 + 2M\sigma_{13}^2 + 2N\sigma_{12}^2 - \overline{\sigma}^2 \tag{3.4}$$

where F, G, H, L, M, and N are constants obtained by tests of the material in different orientations, defined as

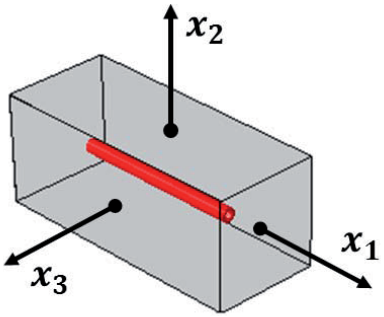

FIG. 4: Material's coordinate system.

$$
\begin{aligned}
F &= \frac{\sigma_0^2}{2}\left(\frac{1}{\overline{\sigma}_{22}^2}+\frac{1}{\overline{\sigma}_{33}^2}-\frac{1}{\overline{\sigma}_{11}^2}\right)=\frac{1}{2}\left(\frac{1}{R_{22}^2}+\frac{1}{R_{33}^2}-\frac{1}{R_{11}^2}\right)\\
G &= \frac{\sigma_0^2}{2}\left(\frac{1}{\overline{\sigma}_{33}^2}+\frac{1}{\overline{\sigma}_{11}^2}-\frac{1}{\overline{\sigma}_{22}^2}\right)=\frac{1}{2}\left(\frac{1}{R_{33}^2}+\frac{1}{R_{11}^2}-\frac{1}{R_{22}^2}\right)\\
H &= \frac{\sigma_0^2}{2}\left(\frac{1}{\overline{\sigma}_{11}^2}+\frac{1}{\overline{\sigma}_{22}^2}-\frac{1}{\overline{\sigma}_{33}^2}\right)=\frac{1}{2}\left(\frac{1}{R_{11}^2}+\frac{1}{R_{22}^2}-\frac{1}{R_{33}^2}\right)
\end{aligned}
\tag{3.5}
$$

$$
L=\frac{3}{2}\left(\frac{\tau_0}{\overline{\sigma}_{23}}\right)^2=\frac{3}{2R_{23}^2},\quad M=\frac{3}{2}\left(\frac{\tau_0}{\overline{\sigma}_{13}}\right)^2=\frac{3}{2R_{13}^2},\quad N=\frac{3}{2}\left(\frac{\tau_0}{\overline{\sigma}_{12}}\right)^2=\frac{3}{2R_{12}^2}
$$

where each $\overline{\sigma}_{ij}$ is the measured yield stress value when σ_{ij} is applied as the only nonzero stress component; σ_0 is the reference yield stress which defines the initial size of the yield surface and τ_0 is the reference shear yield stress defined as $\tau_0 = \sigma_0/\sqrt{3}$. The six yield stress ratios $R_{11} = \overline{\sigma}_{11}/\sigma_0$, $R_{22} = \overline{\sigma}_{22}/\sigma_0$, $R_{33} = \overline{\sigma}_{33}/\sigma_0$, $R_{12} = \overline{\sigma}_{12}/\tau_0$, $R_{13} = \overline{\sigma}_{13}/\tau_0$ and $R_{23} = \overline{\sigma}_{23}/\tau_0$ determine the shape of the anisotropic yield surface which is a truly six-dimensional hypersurface in global stress space. Using matrix notation the yield condition in Eq. (3.4) can be rewritten in the form

$$
\Phi(\boldsymbol{\sigma},\overline{\sigma},\boldsymbol{\alpha})=\frac{1}{2}(\boldsymbol{\sigma}-\boldsymbol{\alpha})^T\boldsymbol{P}(\boldsymbol{\sigma}-\boldsymbol{\alpha})-\overline{\sigma}^2=\frac{1}{2}\boldsymbol{n}^T\boldsymbol{P}\boldsymbol{n}-\overline{\sigma}^2=\boldsymbol{0} \tag{3.6}
$$

where matrix $\boldsymbol{P}$ is defined as

$$
\boldsymbol{P}=\begin{bmatrix}
H+G & -H & -G & 0 & 0 & 0\\
-F & F+H & -H & 0 & 0 & 0\\
-G & -F & G+F & 0 & 0 & 0\\
0 & 0 & 0 & 2N & 0 & 0\\
0 & 0 & 0 & 0 & 2M & 0\\
0 & 0 & 0 & 0 & 0 & 2L
\end{bmatrix} \tag{3.7}
$$

and $\boldsymbol{n} = \boldsymbol{\sigma} - \boldsymbol{\alpha}$ is the relative stress tensor written in vector notation and defined as the difference between the stress $\boldsymbol{\sigma}$ and the back stress $\boldsymbol{\alpha}$. Hill's rate-independent plasticity model postulates an associative plastic flow rule, which is expressed as

$$
\dot{\boldsymbol{\varepsilon}}^p=\dot{\gamma}\frac{\partial\Phi}{\partial\boldsymbol{\sigma}}=\dot{\gamma}\boldsymbol{N}=\dot{\gamma}\boldsymbol{P}\boldsymbol{n} \tag{3.8}
$$

where $\boldsymbol{N} = \boldsymbol{P}\boldsymbol{n}$ is the flow vector and γ is the plastic multiplier. The rate of the accumulated plastic strain can be expressed as

$$
\dot{\overline{\varepsilon}}^p=\sqrt{\frac{2}{3}\left(\dot{\boldsymbol{\varepsilon}}^p\right)^T\boldsymbol{Z}\left(\dot{\boldsymbol{\varepsilon}}^p\right)}=\dot{\gamma}\sqrt{\frac{2}{3}\left(\boldsymbol{P}\boldsymbol{n}\right)^T\boldsymbol{Z}\left(\boldsymbol{P}\boldsymbol{n}\right)} \tag{3.9}
$$

where matrix $\boldsymbol{Z}$ is a compatibility matrix to equate the tensorial contraction to matrix-vectors multiplications. The rate of change of the back stress is supposed to follow Prager's nonlinear kinematic hardening rule which is expressed as

$$\dot{\boldsymbol{\alpha}} = \frac{2}{3} C\left(\overline{\varepsilon}^p\right) \dot{\boldsymbol{\varepsilon}}^p = \dot{\gamma} C\left(\overline{\varepsilon}^p\right) \boldsymbol{P}\boldsymbol{n} \tag{3.10}$$

where $C\left(\overline{\varepsilon}^p\right) = (d\overline{\alpha})/(d\overline{\varepsilon}^p)$ is the kinematic hardening modulus defined by the scalar function $\overline{\alpha}\left(\overline{\varepsilon}^p\right)$ of the accumulated plastic strain. Notice that in Eq. (3.6), $\overline{\sigma}$ is the yield stress value which is also a function of $\overline{\varepsilon}^p$ and $H\left(\overline{\varepsilon}^p\right) = (d\overline{\sigma})/(d\overline{\varepsilon}^p)$ is the isotropic hardening modulus. For materials with kinematic hardening behavior only, $H = 0$ and $\overline{\sigma} \equiv \sigma_0$, meaning that the yield surface size and shape remain constant and only its position is changing according to the kinematic hardening law. Kinematic hardening data can be obtained from simple uniaxial tests in a manner analogous to the determination of the hardening curve for the purely isotropic hardening model. Detailed description of Hill's model definition and implicit stress integration procedure for the corresponding plasticity equations, can be found in Kojić et al. (1996) and Souza (2008).

3.2 Effective Parameters of Hill's Plasticity Model

As a first step in the homogenization procedure, the effective elastic properties of the homogenous CNT-RC are computed. With reference to the material coordinate system of Fig. 4, the homogenized elastic stress–strain relation of an RVE with straight and oriented nanotubes can be expressed by a transversely orthotropic elasticity matrix of the form

$$\begin{bmatrix} \Sigma_{11} \\ \Sigma_{22} \\ \Sigma_{33} \\ \Sigma_{12} \\ \Sigma_{13} \\ \Sigma_{23} \end{bmatrix} = \begin{bmatrix} \mathbb{C}_{1111} & \mathbb{C}_{1122} & \mathbb{C}_{1133} & 0 & 0 & 0 \\ & \mathbb{C}_{2222} & \mathbb{C}_{2233} & 0 & 0 & 0 \\ & & \mathbb{C}_{3333} & 0 & 0 & 0 \\ & & & \mathbb{C}_{1212} & 0 & 0 \\ & sym. & & & \mathbb{C}_{1313} & 0 \\ & & & & & \mathbb{C}_{2323} \end{bmatrix} \begin{bmatrix} E_{11} \\ E_{22} \\ E_{33} \\ E_{12} \\ E_{13} \\ E_{23} \end{bmatrix} \tag{3.11}$$

Notice that nine unknowns components are needed, to fully define the effective elasticity matrix. These components are related with the Young's moduli E_1, E_2, and E_3, associated with directions 1, 2, and 3 of orthotropy respectively, the shear moduli, G_{12}, G_{13}, and G_{23}, associated, respectively, with planes 12, 13, and 23 and satisfying $G_{ij} = G_{ji}$ and three Poisson's ratios ν_{12}, ν_{13}, and ν_{23}. In order to solve for these unknown parameters, four independent Dirichlet's boundary conditions are applied on the RVE, which are derived from the following set of strain deformation cases:

$$\boldsymbol{E} = \left\{ \begin{bmatrix} E_{11} \\ 0 \\ 0 \\ 0 \\ 0 \\ 0 \end{bmatrix}, \begin{bmatrix} 0 \\ E_{22} \\ 0 \\ 0 \\ 0 \\ 0 \end{bmatrix}, \begin{bmatrix} 0 \\ 0 \\ E_{33} \\ 0 \\ 0 \\ 0 \end{bmatrix}, \begin{bmatrix} 0 \\ 0 \\ 0 \\ E_{12} \\ E_{13} \\ E_{23} \end{bmatrix} \right\} \tag{3.12}$$

Substituting the first macrostrain vector in Eq. (3.11), the components $\mathbb{C}_{1111} = \Sigma_{11}/E_{11}$, $\mathbb{C}_{2211} = \Sigma_{22}/E_{11}$, and $\mathbb{C}_{3311} = \Sigma_{33}/E_{11}$ can be directly calculated, while the remaining unknown components of $\mathbb{C}$ are computed in a similar way. Notice here that the response of the RVE is considered linear elastic, as far as the shear stresses developed at the CNT/polymer interface do not violate the ISS of the composite. Thus, in order to calibrate the elastic parameters of the macro constitutive model, the amplitude of the imposed macrostrain has to be lower than the limit point at which slippage of CNTs inside the composite's matrix is initiated.

For the calibration of Hill's plasticity model, the six parameters of Eq. (3.5) along with their corresponding nonlinear kinematic hardening data have to be extracted. Since linear elastic material properties for the matrix and the CNT are assumed, the material nonlinearity of the RVE is attributed solely to CNT slippage at the CNT/polymer interface. Because CNTs are oriented and aligned along the longitudinal direction of the RVE (Fig. 4), only the boundary conditions imposed by the uniaxial strain $\boldsymbol{E} = [E_{11} \;\; 0 \;\; 0 \;\; 0 \;\; 0 \;\; 0]^T$ are sufficient to determine the yield parameters

of Eq. (3.5). Since the aforementioned imposed strains result in multiaxial stress conditions, the yield stress value $\overline{\sigma}_{11}$ of Eq. (3.5) is obtained as the equivalent von Mises stress in the form

$$\overline{\Sigma}_y = \sqrt{\frac{3}{2}\Sigma_{ij}^d \Sigma_{ij}^d} \tag{3.13}$$

where Σ_{ij}^d are the deviatoric components of the effective stress tensor defined by

$$\Sigma_{ij}^d = \Sigma_{ij} - \frac{1}{3}\left(tr\boldsymbol{\Sigma}\right)\delta_{ij} \tag{3.14}$$

The equivalent stress value $\overline{\Sigma}_y$ is calculated by the multiaxial stress states developed in the microstructure at the time instant of slip initiaton. This value corresponds to the initial effective yield stress in the direction of CNT reinforcement. The nonlinear kinematic hardening data are derived by calculating the equivalent yield stresses $\overline{\Sigma}$ as a function of the accumulated plastic strains $\overline{E}^p$ obtained by

$$\overline{E}^p = \sqrt{\frac{2}{3}E_{ij}^p E_{ij}^p} \tag{3.15}$$

where $\boldsymbol{E}^p$ is the plastic strain defined in vector notation as

$$\boldsymbol{E}^p = \boldsymbol{E} - \boldsymbol{E}^e = \boldsymbol{E} - \mathbb{C}^{-1}\boldsymbol{\Sigma} \tag{3.16}$$

For the remaining yield stress parameters of Eq. (3.5), which correspond to the initial yield stresses in the transverse material directions 2 and 3 as these shown in Fig. 4, a large value is assigned in order for material's stresses at these directions to remain inside the elastic domain of Hill's yield surface. This is because at the microsccale interfacial slippage occurs only in the direction of the CNT reinforcement.

4. NUMERICAL RESULTS

The validity of the proposed nonlinear hierarchical multiscale homogenization method is tested in this section by comparing results obtained by FE simulations of the homogenized medium with these of the heterogeneous medium. The results for the heterogeneous medium are obtained through detailed FE discretization of a corresponding microstructure and thus serve as a reference solution. Two test cases are considered. The first corresponds to a microstructured RVE which contains a single straight and oriented CNT and the second consists of a larger CNT-RC specimen reinforced with four CNTs. In both cases validation of the proposed homogenization approach is performed on the basis of sensitivity analysis with respect to various CNT wf and ISS values.

4.1 Test Case 1: Cyclic Test on CNT-RC RVEs

In this example several RVE microstructured FE models containing a single straight and oriented CNT, are subjected to uniaxial cyclic tests and their effective material properties are derived through the proposed homogenization method. These effective properties are subsequently assigned to the corresponding homogenized models. RVEs with wf 0.5, 1, and 2% are constructed by changing only the dimension α of the RVE geometry (see Fig. 5). The RVE length L remains constant at 260 nm and dimension α takes the values 59, 42, and 31 nm in each wf case respectively. The FE mesh of the microstructured model is also shown in Fig. 5 for the highest wf value. The matrix is discretized with 3321, 2009, and 1025 solid elements in each corresponding wf, while a straight CNT with constant length L_{cnt} = 234 nm for all RVEs is discretized with 37 EBEs embedded into the solid elements of the matrix. The basic equations of the embedded element technique have been presented in Savvas et al. (2012). A relative dense discretization of the full length CNT has been chosen in order to accurately capture the variation of interfacial shear stress along the CNT length and provide with an overall accurate prediction of the stick-slip behavior, via the adopted bond-slip model of Section 2.4. The geometry and material properties of the EBEs used here and in all subsequent applications are derived

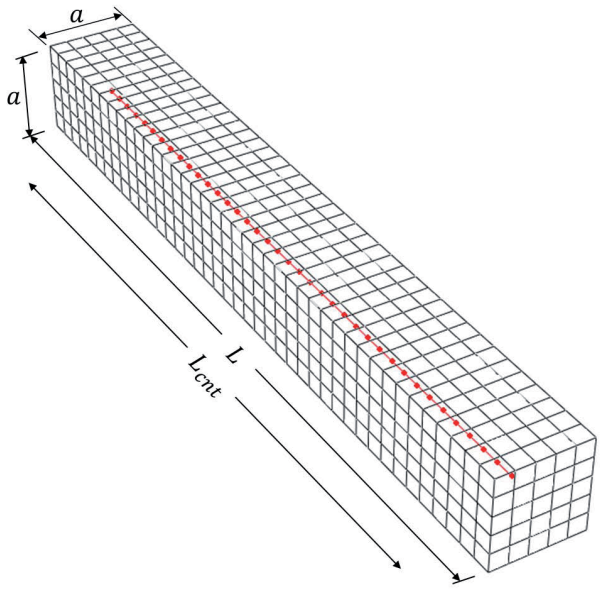

FIG. 5: Geometry and FE mesh of RVE model with straight and oriented CNT.

from a multi-walled CNT with a nominal outer diameter d = 14 nm. This corresponds to an outer single-walled CNT with armchair chirality (100, 100). Using the mMSM approach and the procedure described in Section 2.2, the space frame model of this CNT is reduced to a linear EBE with pipe profile section with wall thickness t = 0.34 nm and mean equivalent diameter d_{eq} = 13.453 nm. Equivalent Young's and shear moduli were calculated from Eqs. (2.3) at $E_{cnt} \simeq 1.051$ TPa and $G_{cnt} \simeq 0.503$ TPa, respectively. The material of the matrix is the semicrystalline thermoplastic polymer poly-ether-ether-ketone (PEEK), which exhibits a Young's modulus E_m = 2.8 GPa, a Poisson's ratio ν_m = 0.4, and an elastic elongation up to 5% (http://www.victrex.com).

A cyclic uniaxial macrostrain $\boldsymbol{E} = [E_{11} \;\; 0 \;\; 0 \;\; 0 \;\; 0 \;\; 0]^T$ was applied with $E_{11} = E_0 \sin(2\pi\nu t)$, E_0 = 5% and ν = 1 Hz. Since elastic elongation of CNTs is more than 6% (Yakobson and Avouris, 2001), the strain amplitude imposed during the cyclic test ensures that both the CNTs and the polymer matrix behave in a linear elastic way. This macrostrain was applied in the form of imposed displacements on the boundary nodes of both micro and macro FE models as follows:

$$\boldsymbol{u}_q = \mathbb{D}_q^T \, \boldsymbol{E} \tag{4.1}$$

where $\boldsymbol{u}_q$ is the dispacement vector on each boundary node q of the RVE FE model and $\mathbb{D}_q$ is a geometrical matrix that depends on the coordinates (x_1, x_2, x_3) of the specific node q in the reference configuration (see Fig. 4) defined as

$$\mathbb{D}_q^T = \begin{bmatrix} x_1 & 0 & 0 & \frac{1}{2}x_2 & 0 & \frac{1}{2}x_3 \\ 0 & x_2 & 0 & \frac{1}{2}x_1 & \frac{1}{2}x_3 & 0 \\ 0 & 0 & x_3 & 0 & \frac{1}{2}x_2 & \frac{1}{2}x_1 \end{bmatrix} \tag{4.2}$$

Figures 6–8 present the stress-strain curves of RVEs with wf = 0.5, 1, and 2%, respectively. In these figures the results of the homogenized model are compared with the reference solution obtained from FE analysis of the micro model, for three different values of the ISS parameter, namely ISS = 40, 80, and 160 MPa. From these figures a very good agreement can be observed in the stress–strain hysteresis loop obtained by the homogenized and the detailed micro model. Specifically, the Bauschinger effect, attributed to the stick-slip mechanism at the CNT/polymer interface,

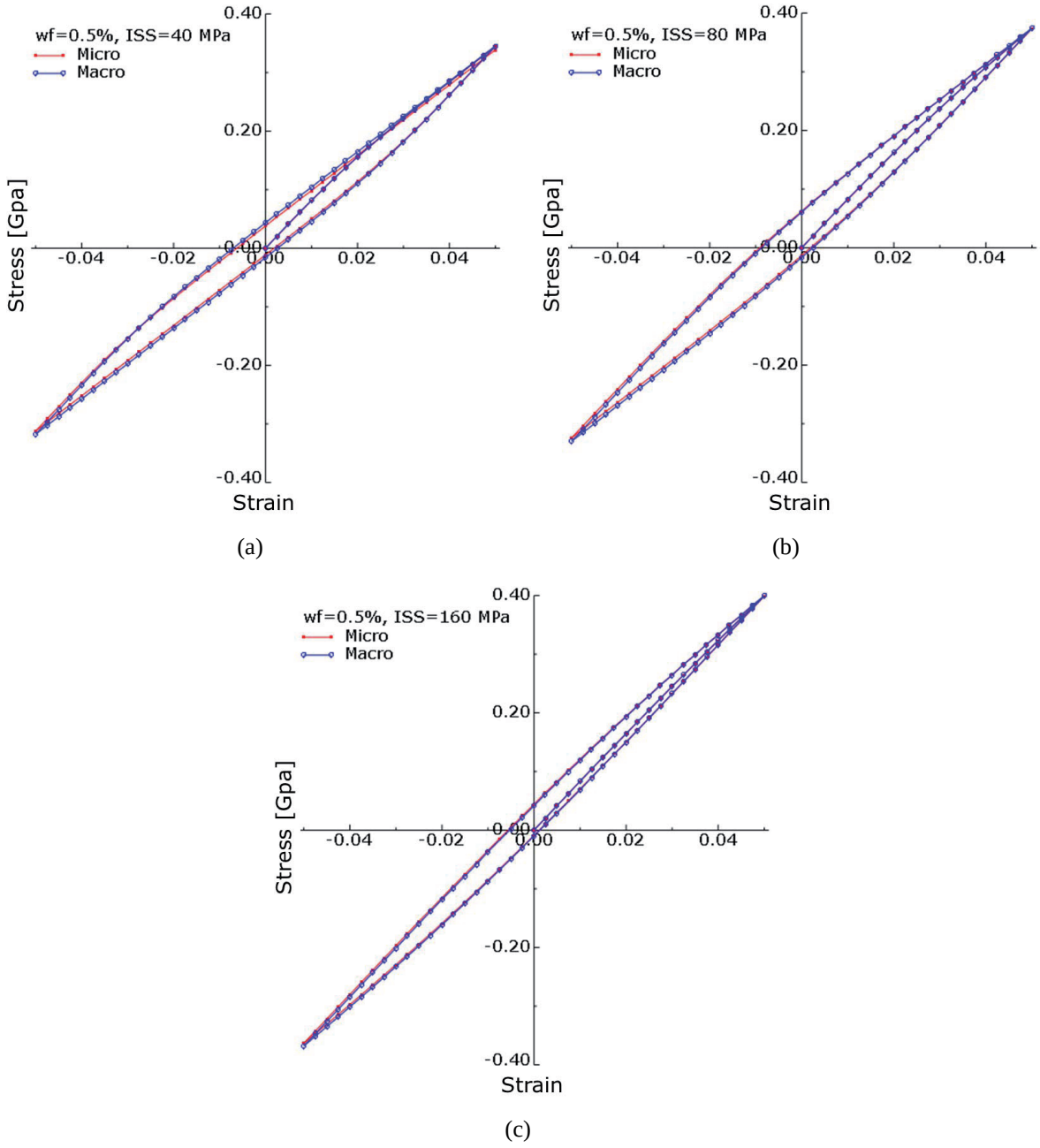

FIG. 6: Comparison of cyclic uniaxial stress-strain curves for micro and macro model with wf = 0.5% and **(a)** ISS = 40 MPa, **(b)** ISS = 80 MPa, and **(c)** ISS = 160 MPa.

is accurately represented by the homogenized model, in which appropriate kinematic hardening data are assigned to the Hill's phenomenological plasticity model, as described in Section 3.2. Small differences on the results observed in some cases may be attributed to calibration errors, especially in establishing the exact initial yield stress point which corresponds to the time instant of slip initiation in the microstructured RVE model.

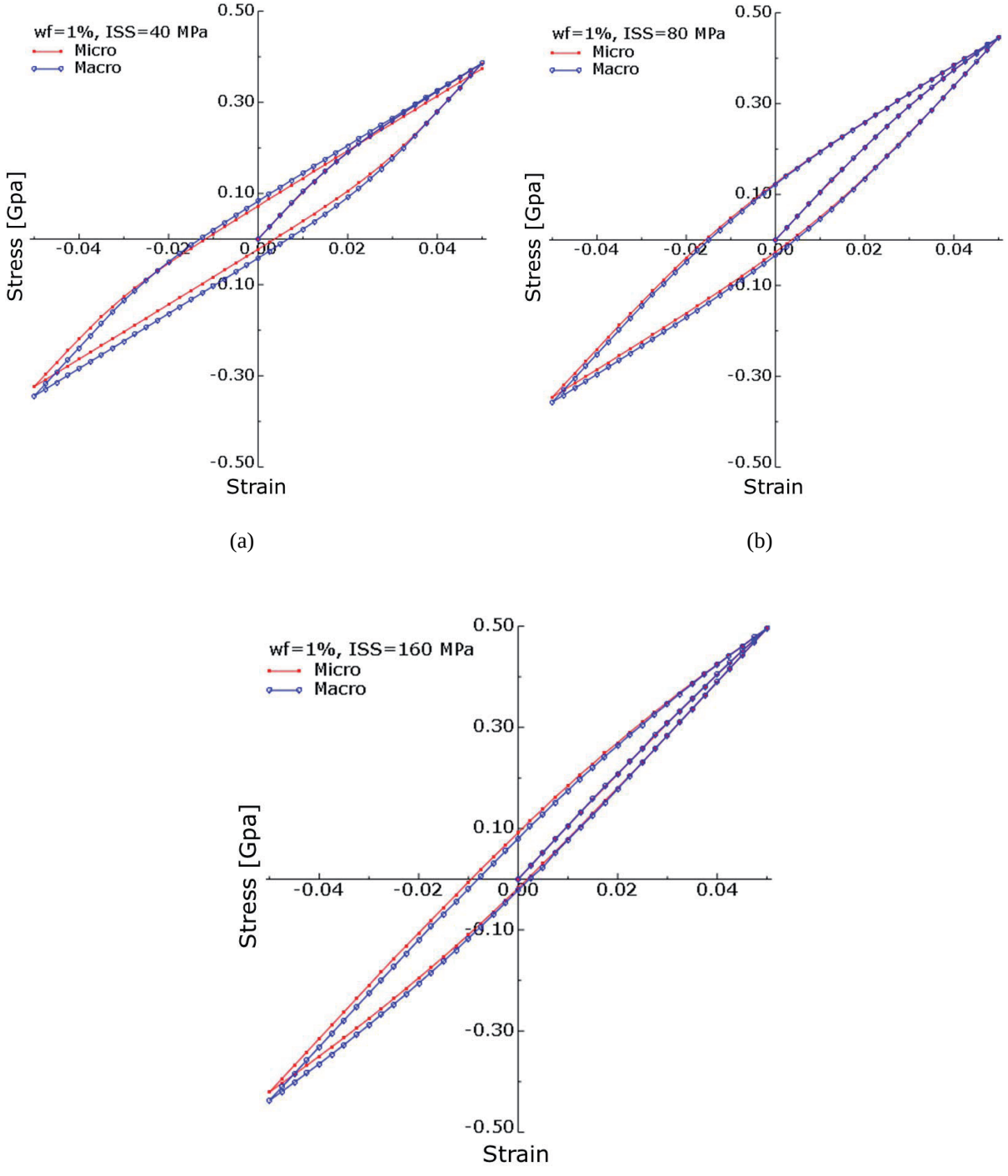

FIG. 7: Comparison of cyclic uniaxial stress-strain curves for micro and macro model with wf = 1% and **(a)** ISS = 40 MPa, **(b)** ISS = 80 MPa, and **(c)** ISS = 160 MPa.

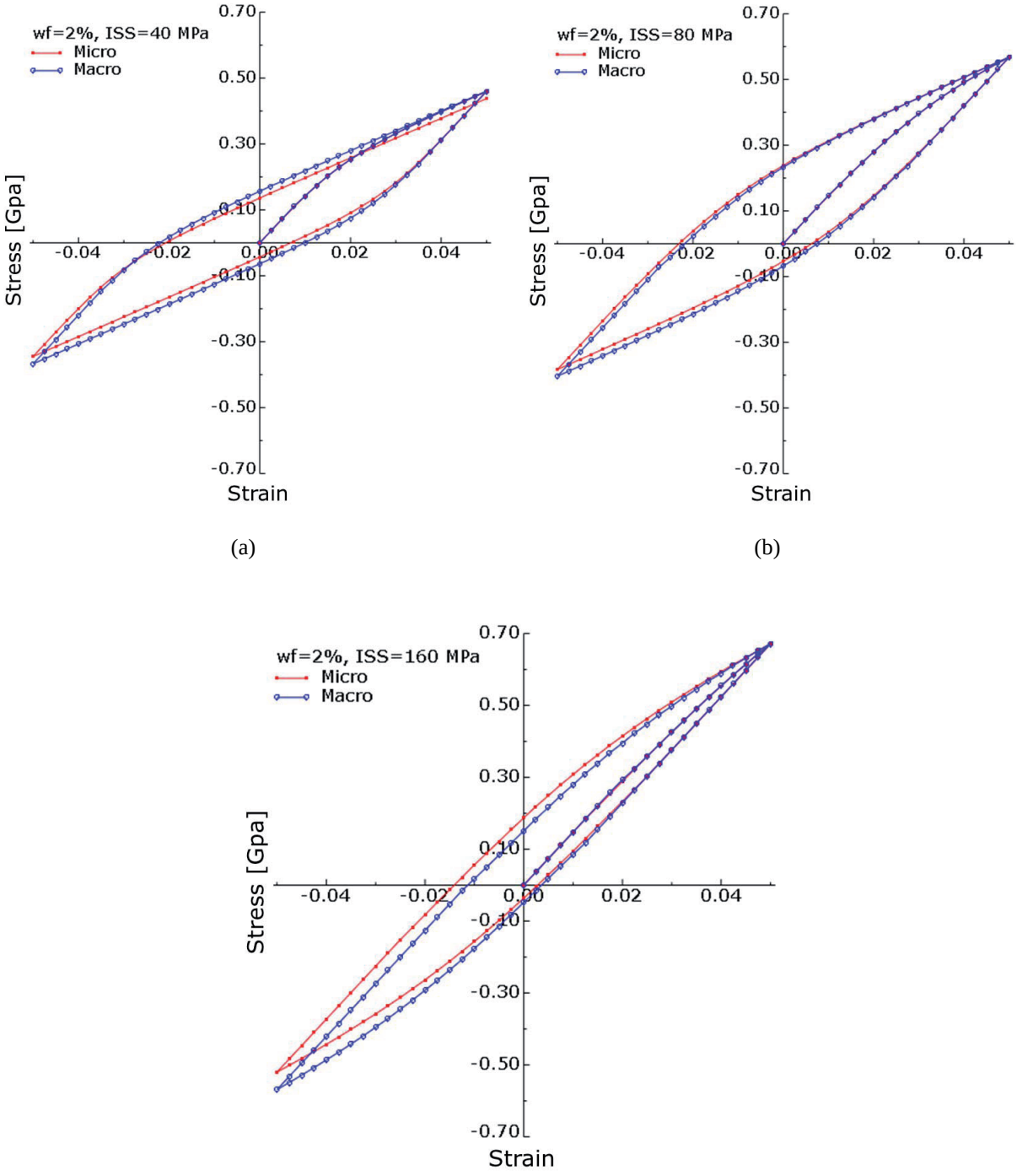

FIG. 8: Comparison of cyclic uniaxial stress-strain curves for micro and macro model with wf = 2% and **(a)** ISS = 40 MPa, **(b)** ISS = 80 MPa, and **(c)** ISS = 160 MPa.

Finally, Figs. 9(a) and 9(b) present the RVEs equivalent hysteretic damping factor ζ_h as a function of the wf and ISS, respectively. This factor is calculated as the ratio of the dissipated to the maximum stored energy per unit cycle and is given by

$$\zeta_h = \frac{D}{\pi \sigma_0 \varepsilon_0} \tag{4.3}$$

where D is the area captured within the hysteresis loop corresponding to the dissipated energy per cycle and σ_0 and ε_0 are the mean stress and strain amplitudes, respectively. From these figures it can be seen that again the homogenized calculated values for ζ_h are close to those obtained by FE analysis on micro models with best correlation occurring for ISS = 80 MPa in all wf cases. Notice that since strain rate effects are not considered in this study, the composite's materials during the cyclic loading remain linear elastic and the energy dissipation of the RVE is attributed solely to CNT/polymer interfacial slippage. In addition, some qualitative conclusions for the damping behavior of the composite can be extracted from the aforementioned plots. Specifically, an increase in the hysteretic damping factor with increasing wf as well as the existence of a peak value for ISS between 80 and 160 MPa regardless of the wf, are observed. Beyond this peak ISS value the hysteretic damping factor drops towards the full-bond condition ($\zeta_h = 0$) where slippage is not present and thus no energy dissipation mechanism exists.

4.2 Test Case 2: Tensile Test on CNT-RC Specimen

A larger FE model of a CNT-RC specimen consisted of a polymer material volume reinforced with four straight and oriented CNTs is examined in this test case. The FE meshes for the heterogenous and the homogenized body are shown in Figs. 10(a) and 10(b), respectively. The wf for this CNT-RC specimen is 2%. The CNTs type and the material properties of those and the matrix are the same with the ones used in test case 1. A monotonic axial tensile load is applied on the boundaries of the specimen in the same way as in the previous example with $E_{11} = E_0 = 5\%$. Figures 11(a)–11(c) present the computed stress–strain curves for both micro and macro models and ISS = 40, 80, and 160 MPa, respectively. As in the previous test case, a very good agreement on the results produced by the two models can be observed for all ISS values. Thus, also in this test case the homogenized model can accurately reproduce the material nonlinearity induced by the microslippage at the CNT/polymer interface.

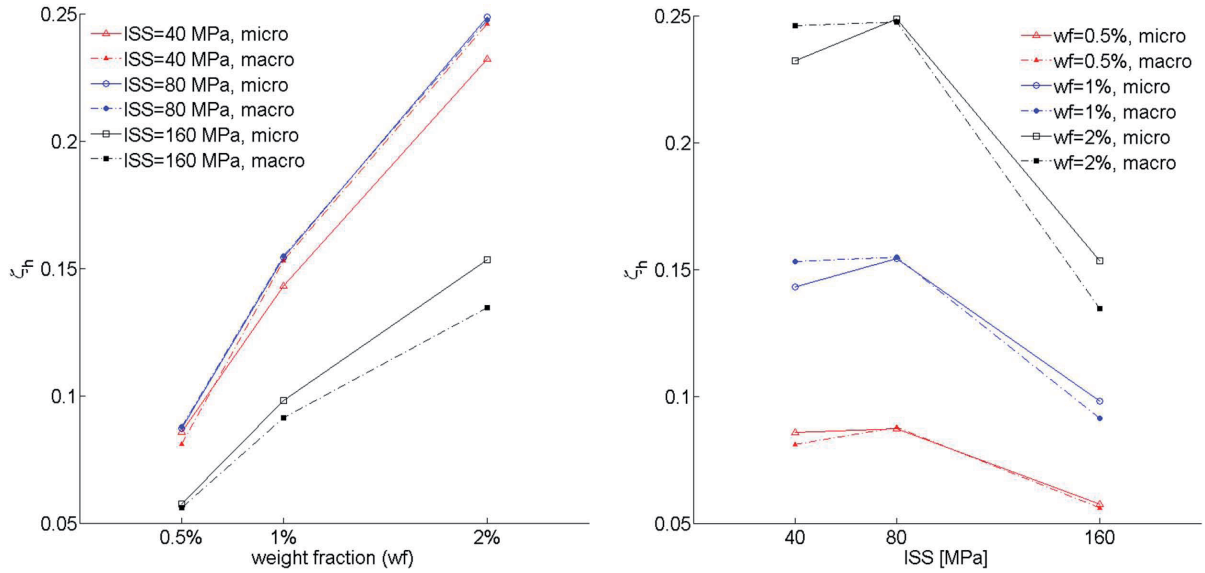

FIG. 9: Equivalent hysteretic damping factor ζ_h for RVEs as a function of **(a)** wf and **(b)** ISS values.

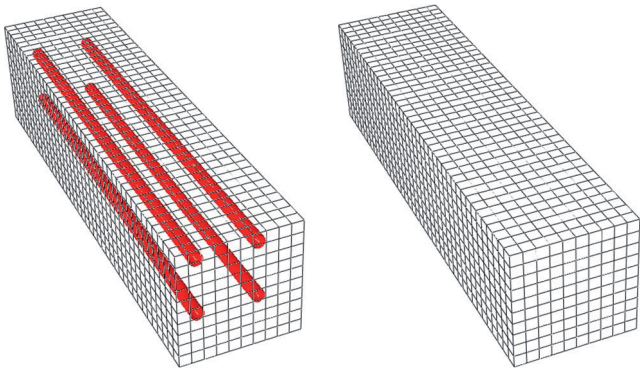

(a) (b)

FIG. 10: FE mesh of CNT-RC specimen for **(a)** heterogenous and **(b)** homogenized model.

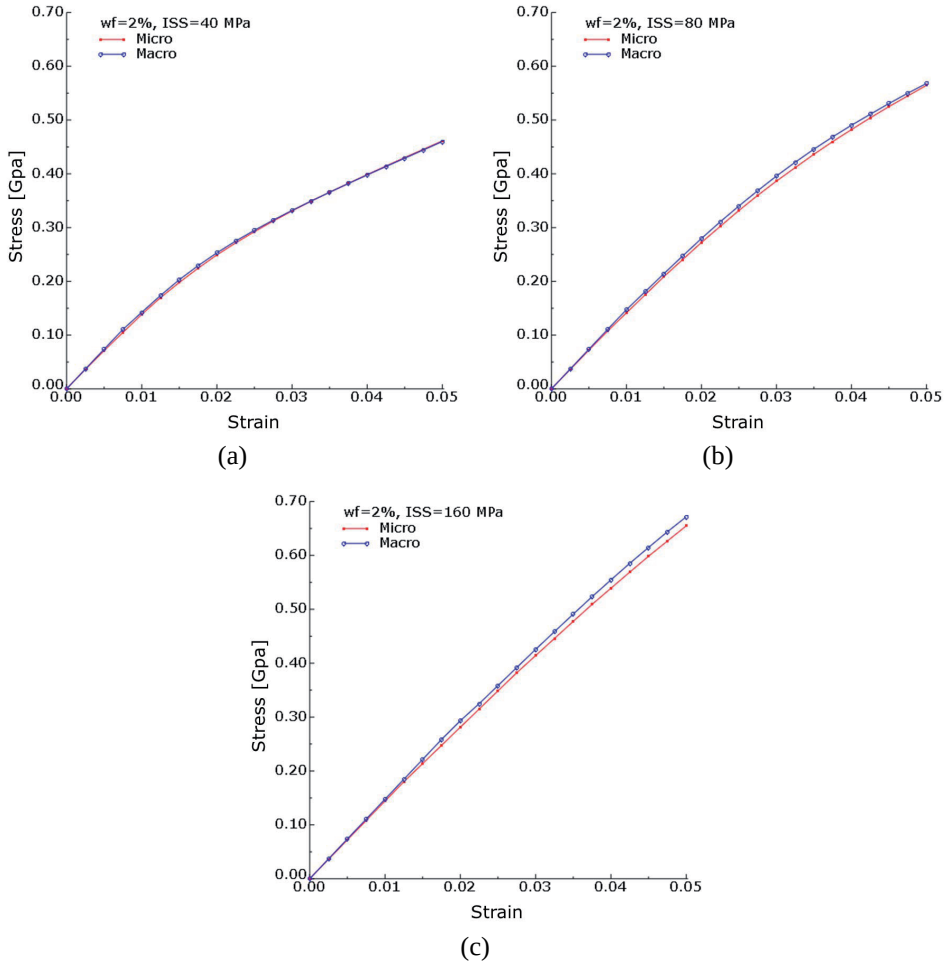

FIG. 11: Comparison of uniaxial monotonic stress-strain curves for heterogenous and homogenized model with wf = 2% and **(a)** ISS = 40 MPa, **(b)** ISS = 80 MPa, and **(c)** ISS = 160 MPa.

5. CONCLUSIONS

A nonlinear hierarchical multiscale approach is proposed in this work, for the characterization of the mechanical and damping properties of CNT-RCs considering slippage at CNT/polymer interface. The proposed numerical strategy encompasses various length scales, from nano to micro to macro. Individual CNTs are modeled at the nanoscale as space frame structures using the mMSM approach and projected to EBEs which form long straight CNT "ropes" at the microscale. Then these CNTs are embedded in a polymer matrix to construct the microstructured RVEs. A nonlinear homogenization scheme is implemented in order to compute effective material properties for the macrocontinuum based on Hill's orthotropic plasticity theory. From the comparison of the results produced by the microstructured and the homogenized FE models it is concluded that the proposed multiscale homogenization strategy is capable to accurately represent the transversely orthotropic material nonlinearity of CNT-RCs induced by the microslippage at the CNT/polymer interface. The effect of random CNT orientation as well as waviness on the nonlinear effective material properties of the CNT-RCs, not taken into account in the present study, is a subject for future work.

ACKNOWLEDGMENTS

This research investigation was performed under the European Commission project NMP4-LA-2010-246067, Acronym: M-RECT and the European Research Council Advanced Grant "MASTER Mastering the computational challenges in numerical modeling and optimum design of CNT reinforced composites" (ERC-2011-ADG 20110209). The European financial support is strongly acknowledged.

REFERENCES

Andrews, R. and Weisenberger, M., Carbon nanotube polymer composites, *Curr. Opin. Solid State Mater. Sci.*, vol. **8**, no. 1, pp. 31–37, 2004.

Arroyo, M. and Belytschko, T., Finite crystal elasticity of carbon nanotubes based on the exponential Cauchy-Born rule, *Phys. Rev. B*, vol. **69**, p. 115415, 2004.

Barber, A. H., Cohen, S. R., and Wagner, H. D., Measurement of carbon nanotube–polymer interfacial strength, *Appl. Phys. Lett.*, vol. **82**, no. 23, pp. 4140–4142, 2003.

Chang, T. and Gao, H., Size-dependent elastic properties of a single-walled carbon nanotube via a molecular mechanics model, *J. Mech. Phys. Solids*, vol. **51**, no. 6, pp. 1059–1074, 2003.

Chen, W. and Tao, X., Production and characterization of polymer nanocomposite with aligned single wall carbon nanotubes, *Appl. Surf. Sci.*, vol. **252**, no. 10, pp. 3547–3552, 2006.

Chen, W.-H., Cheng, H.-C., and Liu, Y.-L., Radial mechanical properties of single-walled carbon nanotubes using modified molecular structure mechanics, *Comput. Mater. Sci.*, vol. **47**, no. 4, pp. 985–993, 2010.

Demczyk, B., Wang, Y., Cumings, J., Hetman, M., Han, W., Zettl, A., and Ritchie, R., Direct mechanical measurement of the tensile strength and elastic modulus of multiwalled carbon nanotubes, *Mater. Sci. Eng.: A*, vol. **334**, no. 12, pp. 173–178, 2002.

Dumitrica, T., Belytschko, T., and Yakobson, B. I., Bond-breaking bifurcation states in carbon nanotube fracture, *J. Chem. Phys.*, vol. **118**, no. 21, pp. 9485–9488, 2003.

Frankland, S. J. V., Caglar, A., Brenner, D. W., and Griebel, M., Molecular simulation of the influence of chemical cross-links on the shear strength of carbon nanotube-polymer interfaces, *J. Phys. Chem. B*, vol. **106**, no. 12, pp. 3046–3048, 2002.

Ganesan, Y., Peng, C., Lu, Y., Loya, P. E., Moloney, P., Barrera, E., Yakobson, B. I., Tour, J. M., Ballarini, R., and Lou, J., Interface toughness of carbon nanotube reinforced epoxy composites., *ACS Appl. Mater. Interfaces*, vol. **3**, no. 2, p. 129, 2011.

Griebel, M. and Hamaekers, J., Molecular dynamics simulations of the elastic moduli of polymer-carbon nanotube composites, *Comput. Methods Appl. Mech. Eng.*, vol. **193**, no. 1720, pp. 1773–1788, 2004.

Han, Y. and Elliott, J., Molecular dynamics simulations of the elastic properties of polymer/carbon nanotube composites, *Comput. Mater. Sci.*, vol. **39**, no. 2, pp. 315–323, 2007.

Hashin, Z., Analysis of composite materials, *J. Appl. Mech.*, vol. **50**, no. 2, pp. 481–505, 1983.

Hehre, W. J., *A Guide to Molecular Mechanics and Quantum Chemical Calculations*, Wavefunction, Irvine, CA, 2003.

Hill, R., *Mathematical Theory of Plasticity*, Clarendon Press, London, 1950.

Hill, R., Elastic properties of reinforced solids: Some theoretical principles, *J. Mech. Phys. Solids*, vol. **11**, no. 5, pp. 357–372, 1963.

Hou, Y., Tang, J., Zhang, H., Qian, C., Feng, Y., and Liu, J., Functionalized few-walled carbon nanotubes for mechanical reinforcement of polymeric composites, *ACS Nano*, vol. **3**, no. 5, pp. 1057–1062, 2009.

Iijima, S., Helical microtubules of graphitic carbon, *Nature*, vol. **354**, pp. 56–58, 1991.

Jin, Y. and Yuan, F., Simulation of elastic properties of single-walled carbon nanotubes, *Compos. Sci. Technol.*, vol. **63**, no. 11, pp. 1507–1515, 2003.

Kojić, M., Grujović, N., Slavković, R., and Živković, M., A general orthotropic von mises plasticity material model with mixed hardening: Model definition and implicit stress integration procedure, *J. Appl. Mech.*, vol. **63**, p. 376, 1996.

Kouznetsova, V., Geers, M., and Brekelmans, W., Multi-scale second-order computational homogenization of multi-phase materials: a nested finite element solution strategy, *Comput. Methods Appl. Mech. Eng.*, vol. **193**, no. 48, pp. 5525–5550, 2004.

Lau, A. K.-T. and Hui, D., The revolutionary creation of new advanced materials-carbon nanotube composites, *Compos. Part B: Eng.*, vol. **33**, no. 4, pp. 263–277, 2002.

Li, C. and Chou, T.-W., Elastic moduli of multi-walled carbon nanotubes and the effect of van der waals forces, *Compos. Sci. Technol.*, vol. **63**, no. 11, pp. 1517–1524, 2003a.

Li, C. and Chou, T.-W., A structural mechanics approach for the analysis of carbon nanotubes, *Int. J. Solids Struct.*, vol. **40**, no. 10, pp. 2487–2499, 2003b.

Maugin, G., *The Thermomechanics of Plasticity and Fracture*, vol. 7, Cambridge University Press, Cambridge, 1992.

Miehe, C. and Koch, A., Computational micro-to-macro transitions of discretized microstructures undergoing small strains, *Arch. Appl. Mech.*, vol. **72**, pp. 300–317, 2002.

Namilae, S. and Chandra, N., Multiscale model to study the effect of interfaces in carbon nanotube-based composites, *J. Eng. Mater. Technol.*, vol. **127**, no. 2, pp. 222–232, 2005.

Odegard, G., Gates, T., Wise, K., Park, C., and Siochi, E., Constitutive modeling of nanotube-reinforced polymer composites, *Compos. Sci. Technol.*vol. **63**, no. 11, pp. 1671–1687, 2003.

Park, H., Zhao, J., and Lu, J. P., Effects of sidewall functionalization on conducting properties of single wall carbon nanotubes, *Nano Lett.*, vol. **6**, no. 5, pp. 916–919, 2006.

Qian, D., Dickey, E. C., Andrews, R., and Rantell, T., Load transfer and deformation mechanisms in carbon nanotube-polystyrene composites, *Appl. Phys. Lett.*, vol. **76**, no. 20, pp. 2868–2870, 2000.

Qian, D., Liu, W. K., and Zheng, Q., Concurrent quantum/continuum coupling analysis of nanostructures, *Comput. Methods Appl. Mech. Eng.*, vol. **197**, no. 41, pp. 3291–3323, 2008.

Salvetat, J.-P., Bonard, J.-M., Thomson, N., Kulik, A., Forr, L., Benoit, W., and Zuppiroli, L., Mechanical properties of carbon nanotubes, *Appl. Phys. A*, vol. **69**, pp. 255–260, 1999.

Savvas, D., Papadopoulos, V., and Papadrakakis, M., The effect of interfacial shear strength on damping behavior of carbon nanotube reinforced composites, *Int. J. Solids Struct.*, vol. **49**, no. 26, pp. 3823–3837, 2012.

Schadler, L. S., Giannaris, S. C., and Ajayan, P. M., Load transfer in carbon nanotube epoxy composites, *Appl. Phys. Lett.*, vol. **73**, no. 26, pp. 3842–3844, 1998.

Seidel, G. D. and Lagoudas, D. C., Micromechanical analysis of the effective elastic properties of carbon nanotube reinforced composites, *Mech. Mater.*, vol. **38**, no. 8-10, pp. 884–907, 2006.

Shen, J., Huang, W., Wu, L., Hu, Y., and Ye, M., The reinforcement role of different amino-functionalized multi-walled carbon nanotubes in epoxy nanocomposites, *Compos. Sci. Technol.*, vol. **67**, no. 15–16, pp. 3041–3050, 2007.

Souza, E. N., *Computational Methods for Plasticity: Theory and Applications*, John Wiley and Sons, Ltd, Publication, New York, 2008.

Spanos, P. and Kontsos, A., A multiscale Monte Carlo finite element method for determining mechanical properties of polymer nanocomposites, *Probab. Eng. Mech.*, vol. **23**, no. 4, pp. 456–470, 2008.

Thostenson, E. T., Li, C., and Chou, T.-W., Nanocomposites in context, *Compos. Sci. Technol.*, vol. **65**, no. 3-4, pp. 491–516, 2005.

van der Sluis, O., Schreurs, P., and Meijer, H., Effective properties of a viscoplastic constitutive model obtained by homogenisation,

Mech. Mater., vol. **31**, no. 11, pp. 743–759, 1999.

Wang, S., Liang, R., Wang, B., and Zhang, C., Load-transfer in functionalized carbon nanotubes/polymer composites, *Chem. Phys. Lett.*, vol. **457**, no. 4-6, pp. 371–375, 2008.

Wang, Y., Xu, Z., Chen, L., Jiao, Y., and Wu, X., Multi-scale hybrid composites-based carbon nanotubes, *Polym. Compos.*, vol. **32**, no. 2, pp. 159–167, 2011.

Weinan, E., Engquist, B., Xiantao, L., Weiqing, R., and Vanden-Eijnden, E., Heterogeneous multiscale methods: A review, *Commun. Comput. Phys.*, vol. **2**, no. 3, pp. 367–450, 2007.

Wernik, J. and Meguid, S. A., Coupling atomistics and continuum in solids: Status, prospects, and challenges, *Int. J. Mech. Mater. Design*, vol. **5**, no. 1, pp. 79–110, 2009.

Xiao, J., Gama, B., and Gillespie, J., An analytical molecular structural mechanics model for the mechanical properties of carbon nanotubes, *Int. J. Solids Struct.*, vol. **42**, no. 11-12, pp. 3075–3092, 2005.

Xu, Y., Ray, G., and Abdel-Magid, B., Thermal behavior of single-walled carbon nanotube polymer-matrix composites, *Compos. Part A: Appl. Sci. Manuf.*, vol. **37**, no. 1, pp. 114–121, 2006.

Yakobson, B. I. and Avouris, P., Mechanical properties of carbon nanotubes, *Carbon Nanotubes*. Springer, Berlin, pp. 287–327, 2001.

Yang, M., Koutsos, V., and Zaiser, M., Interactions between polymers and carbon nanotubes: A molecular dynamics study, *J. Phys. Chem. B*, vol. **109**, no. 20, pp. 10009–10014, 2005.

Yang, S., Yu, S., Kyoung, W., Han, D.-S., and Cho, M., Multiscale modeling of size-dependent elastic properties of carbon nanotube/polymer nanocomposites with interfacial imperfections, *Polymer*, vol. **53**, no. 2, pp. 623–633, 2012.

Yuen, S.-M., Ma, C.-C. M., Wu, H.-H., Kuan, H.-C., Chen, W.-J., Liao, S.-H., Hsu, C.-W., and Wu, H.-L., Preparation and thermal, electrical, and morphological properties of multiwalled carbon nanotubeand epoxy composites, *J. Appl. Polym. Sci.*, vol. **103**, no. 2, pp. 1272–1278, 2007.

Zhang, D.-B. and Dumitrica, T., Elasticity of ideal single-walled carbon nanotubes via symmetry-adapted tight-binding objective modeling, *Appl. Phys. Lett.*, vol. **93**, no. 3, p. 031919, 2008.